minerals

MDPI

Article

Trace Elements in Silicate Minerals of the Kargapole Meteorite

Kristina Sukhanova [1,*], Sergey Skublov [1,2], Alexandra Gavrilchik [2] and Olga Galankina [1]

[1] Institute of Precambrian Geology and Geochronology, Russian Academy of Sciences, 199034 St. Petersburg, Russia
[2] Saint Petersburg Mining University, 199106 St. Petersburg, Russia
* Correspondence: cris.suhanova92@yandex.ru

Abstract: The aim of the present contribution was to evaluate the trace element mobility in olivine, low-Ca pyroxene and plagioclase of the Kargapole meteorite under thermal or impact metamorphic conditions and recognition of the properties of chondrule-forming events. The compositions of the minerals were analyzed using an electron probe microanalyser (EPMA) and a secondary ion mass spectrometer (SIMS). No considerable deviations in the trace element concentrations of olivine and pyroxene from unequilibrated ordinary chondrites in the Kargapole meteorite were revealed. This points to minor effects of impact metamorphism and terrestrial weathering on trace element mobilization. Olivine and low-Ca pyroxene of porphyritic olivine-pyroxene chondrule POP-0 contain higher trace element concentrations than minerals in porphyritic olivine PO-2 and olivine-pyroxene POP-4 chondrules and in the meteorite matrix.

Keywords: meteorites; equilibrated ordinary chondrites; trace elements; olivine; pyroxene; plagioclase

Citation: Sukhanova, K.; Skublov, S.; Gavrilchik, A.; Galankina, O. Trace Elements in Silicate Minerals of the Kargapole Meteorite. *Minerals* **2023**, *13*, 368. https://doi.org/10.3390/min13030368

Academic Editor: Yang Liu

Received: 24 January 2023
Revised: 23 February 2023
Accepted: 1 March 2023
Published: 6 March 2023

1. Introduction

Extraterrestrial material on the Earth occurs mainly as fragments of equilibrated ordinary chondrites (EOC). EOCs consist of silicate spherules (chondrules), less than 1 mm in diameter, produced by rapid cooling of melt droplets in a solar nebula. EOCs have never experienced core-mantle differentiation and segregation, and retain the chemical properties of pristine matter. However, as a result of thermal metamorphism on the chondritic parent bodies, the major element composition of EOC minerals is partly (petrographic EOC types 4 and 5) or completely (type 6) equilibrated [1].

The trace element concentration of chondrite minerals can provide new information on conditions of EOC formation. The analysis of the composition of refractory trace elements in olivine, pyroxene and glass of chondrules in unequilibrated ordinary chondrites (UOC) has revealed various types of crystallization of porphyric chondrules and has made it possible to estimate their relative cooling rates [2–4]. The composition of moderately volatile trace elements usually indicates the interaction of a chondrule with surrounding gas in a nebula [5,6]. The trace element composition of matrix minerals is analyzed to detect the formation of minerals under protoplanetary disk conditions similar to or different from those of chondrules [7].

Earlier studies of trace elements in the silicate minerals of EOC failed to show evidence of trace element homogenization [8–11]. However, in addition to having experienced thermal metamorphism, EOCs may be partly molten upon impact events and become subject to weathering under terrestrial conditions. In this study, we assessed the effect of these processes on silicate mineral compositions in the porphyric chondrules of the Kargapole equilibrated ordinary chondrite (H4).

The Kargapole meteorite was found in July 1961 in the Kargapole District, Kurgan Region, Russia, by A.S. Okhapkin, a local resident. The meteorite, split in half, lay in a meadow in a 10 cm deep pit overgrown with grass. Okhapkin's attention was drawn by the unusual molten surface and dark-brown color of the stone. It was carried to the

town of Udarnik and kept under a shed for two years. In 1963, the Uralian Commission for Meteorites announced that the stone had come from outer space and named it the Kargapole meteorite [12]. The larger fragment of the meteorite was sent to the USSR Committee for Meteorites and the smaller fragment is exhibited in the Uralian Geological Museum [13].

In 1966, an in-depth study of the Kargapole meteorite was carried out. Its appearance, size, basic minerals (olivine, enstatite, plagioclase, troilite, native iron, chromite, and magnetite), fusion crust and hypergene minerals (goethite, bravoite, iddingsite, and kaolinite) were described, the chemical compositions of the minerals and meteorite were analyzed, the specific gravity and microporosity of the meteorite were calculated, and its absolute age of 4.25 ± 0.15 Ga was estimated using the K-Ar method [12]. However, this age is probably too young due to preferential Ar loss during impact events on parent body or in space.

Silicate chondrules in the Kargapole meteorite are mainly barred, radial and microporphyric types varying in size from 0.2 to 1.2 mm. Chromite chondrules are smaller (up to 0.3 mm in diameter) and are much scarcer than silicate chondrules. It was emphasized in the description that the meteorite was highly weathered and highly shattered, and that its hypergene minerals were abundant [12]. Chemical analysis showed that the meteorite belongs to the group of olivine-bronzite chondrites [14].

A high degree of weathering of the meteorite Is responsible for its low thermal luminescent intensity [15], increased natural remanent magnetization [16], and the decrease of meteorite mass upon heating [17].

In 2015, the Kargapole meteorite was found to contain pentlandite, and its chemical composition and morphology were described [18,19]. In 2017, additional minerals, such as diopside, tetrataenite, chromian spinel, chlorapatite and merrilite, were described for the first time from the meteorite [20].

The peak temperature of thermal metamorphism on the parent chondritic body, obtained using an olivine-Cr spinel geothermometer, approaches 690 °C, which is characteristic of chondrites of petrographic type 5, but in this case it could be due to the disturbance of equilibrium by impact metamorphism experienced by the meteorite [21].

2. Materials and Methods

In this study, the major element composition of minerals was determined using the electron probe micro analyzer (EPMA) at the Institute of Precambrian Geology and Geochronology Russian Academy of Sciences (IPGG RAS) on a Jeol JXA-8230. This electron probe microanalyzer was equipped with three wavelength dispersive spectrometers. Point measurements of mineral composition were performed at an accelerating voltage of 20 kV and a current of 20 nA for olivine and pyroxene, and at a current of 10 nA for plagioclase. The focused beam was 3 μm in diameter. Natural minerals, as well as pure oxides and metals, were used as standards. To correct the matrix effect, the ZAF algorithm was used. The Kα1 lines were measured for all elements.

The bulk chemical composition of the chondrules and matrix at the major element level was analyzed by SEM-EDS at IPGG RAS on a JEOL JSM-6510LA scanning electron microscope with a JED-2200 energy dispersion attachment. Meteorite fragments were placed into a standard epoxy mount, polished and covered in carbon. The bulk composition of the chondrules and meteorite matrix were analyzed over a chondrule's area with an accelerating voltage of 20 kV and a current of 1 nA. The accumulation time of each spectrum was 70 s. Natural minerals, as well as pure oxides and metals, were used as standards. The ZAF algorithm was used to correct the matrix effect.

The trace element, including rare-earth element (REE), concentrations of minerals were measured by secondary ion mass-spectrometry (SIMS) using a Cameca IMS-4f ion microprobe at the Yaroslavl Branch of the Valiev Institute of Physics and Technology, Russian Academy of Sciences (YaF FTIAN), following the procedure described in [22–24]. Prior to measurements, the mount was sputtered with gold. A survey was conducted employing this ion microprobe under the following conditions: a primary ion beam O_2^-,

beam diameter of 20 μm; ion current of 5–7 nA; and accelerating voltage of the primary beam of 15 kV. Positive secondary ions were collected from an area of 20 μm in diameter, limited by a field aperture. Molecular and cluster ions were energy filtered using an offset voltage of −100 V, with an energy window of 50 eV. Five counting cycles were carried out with a discrete transition between mass peaks within the given set. The accumulation time varied depending on signal intensity and was determined automatically by statistical control. The maximum counting time for any species in each cycle was 30 s. Counting time was dynamically corrected for each element and varied between 5 and 120 s depending on current counting statistics. Single analyses are averaged from 3 cycles of measurements. Total analysis time varied from 50 to 70 min.

The absolute concentrations of each element were calculated from the measured intensities of positive single-atom secondary ions, which were normalized to the intensity of secondary $^{30}Si^{+}$ ions, using the relative sensitivity factors $C_i = I_i/I^{30}Si \times {}_i \times C_{SiO2}$. Calibration curves were based on the measurements of the set of well-characterized standard samples [25]. The signals of $^{153}Eu^{+}$, $^{174}Yb^{+}$, $^{158}Gd^{+}$, and $^{167}Er^{+}$ were corrected to the interfering oxides of Ba and lighter REE in accordance to the scheme reported by Bottazzi et al. [26]. Glass KL-2G [25,27] and NIST-610 [28] were used as daily monitors for trace element analyses. Accuracy and precision were estimated to be better than 10% for all elements with contents above 1 ppm and 10% to 30% for contents of 0.1–1 ppm. The detection limit for almost all elements was about 0.01 ppm [22,29]. The trace element composition of rock-forming minerals was analyzed as close as possible to the analytical points for major elements using the EPMA method. The REE patterns of minerals were normalized to CI chondrite [30].

3. Results

The petrographic study of the meteorite revealed porphyric- and bar-structured chondrules. The porphyric chondrules, approximately 1 mm in diameter, are rounded, have no metallic rims, are highly porous and have fractures along the chondrule boundary. The porphyric chondrules consist of coarse idiomorphic olivine and pyroxene crystals and contain practically no plagioclase. The drop-shaped barred chondrules are smaller (approximately 0.5 mm in diameter) and contain metallic rims and veins. The barred chondrules consist of thin pyroxene bars and have practically no plagioclase in chondrules. The meteorite contains a multi-bar aggregate consisting of four differently oriented pyroxene barred chondrules.

The meteorite matrix is composed of coarse-grained olivine and pyroxene grains, as well as tiny plagioclase aggregates. Kamacite, taenite and troilite form coarse metallic aggregates growing on olivine and pyroxene grains and occasionally occur as metallic veins or single fine grains in chondrules. Chromite and tetrataenite occasionally occur in metallic aggregates, but are scarcer. Secondary minerals, similar in composition to trevorite (Fe 33 wt.%, Ni 21 wt.%, O 37 wt.%), evolve after kamacite and taenite. In addition, present in the meteorite matrix along the silicate-metallic mineral boundary are xenomorphic merrilite and apatite grains measuring 200 to 500 μm. The meteorite matrix displays an abundance of kamacite- and taenite-filled fractures; melting pockets are occasionally encountered.

Olivine in the Kargapole meteorite commonly occurs in chondrules and matrix as coarse (250–500 μm) idiomorphic phenocrysts. Olivine corresponds to forsterite ($Fo_{78–80}$) and has a similar major element composition in chondrules and the meteorite matrix. Some coarse olivine crystals in porphyric chondrules are highly corroded or highly fractured.

Pyroxenes in the meteorite occur as low and high-Ca types, such as enstatite and diopside, respectively. Enstatite (Fs_{17}, Wo_1) is widespread as hypidiomorphic grains in the porphyric chondrules and the meteorite matrix, and also intergrown with diopside. Sometimes enstantite forms barred chondrules. Diopside (Fs_6, Wo_{48}) in the meteorite occurs only intergrown with enstatite. No independent high-Ca pyroxene grains have been observed. The composition of low-Ca pyroxene in Kargapole meteorite is the same in chondrules and the meteorite matrix.

Plagioclase fills interstices between olivine and pyroxene in the chondrules and the meteorite matrix. Plagioclase is oligoclase with a composition An_{13}, Or_5; its composition is homogeneous and constant. Plagioclase aggregates are 50 μm in size and are scarce.

Kamacite (Ni 6.7 wt.%) and taenite (Ni 33.0 wt.%) often occur in the meteorite matrix, forming coarse (250–500 μm) xenomorphic aggregates, overgrowing idiomorphic olivine or pyroxene crystals or forming rims around meteorite chondrules. A tetrataenite phase (Ni 55.5 wt.%) in taenite-kamacite intergrowths is occasionally encountered. Fine (10–20 μm) kamacite and taenite grains sometimes occur in the chondrules. Approximately 40%–60% of the coarsest kamacite and taenite aggregates are replaced by unidentified secondary minerals.

Troilite forms coarse (200–500 μm) intergrowths with kamacite, taenite, or chromite. Separate troilite aggregates vary markedly in size and look highly heterogeneous in a BSE-regime. Troilite is most commonly present at the chondrule boundary, and less commonly in the meteorite matrix.

Chromite is intergrown with kamacite and troilite in the meteorite matrix. Xenomorphic chromite aggregates are 100–150 μm in size.

The previously mentioned melting pockets and an abundance of troilite veins suggest that the Kargapole meteorite was subjected to impact metamorphism corresponding to impact stage S4 and an impact pressure of 25–30 GPa [1]. The presence of secondary minerals replacing 40%–60% of kamacite and taenite grains indicates stage W2 of terrestrial weathering [31].

The three coarsest porphyric chondrules 1POP-0, 1PO-2, and 1POP-4 in the Kargapole meteorite sample were studied. Chondrules 1POP-0 and 1POP-4 are about 1 mm in diameter, have no metallic rim, and are highly porous. The chondrules consist of olivine and enstatite crystals with interstices filled with plagioclase. Chondrule 1PO-2 is 0.5 mm in size and has a continuous kamacite-taenite rim. This chondrule consists almost entirely of olivine grains overgrown with enstatite along the chondrule rim.

The three chondrules in general have similar major element compositions, but chondrules 1POP-0 and 1POP-4 contain more Ca than 1PO-2 (Table 1). High Ca concentrations could be due to the presence of high-Ca pyroxene (diopside), which overgrows coarse enstatite grains. The meteorite matrix contains more moderately volatile elements (Mn, Na, K, and Ni) than the chondrules.

Table 1. Bulk composition (in wt.%) of chondrules and matrix from the Kargapole (H4) meteorite.

	1POP-0		**1PO-2**		**1POP-4**	
	Chondrule	**Matrix**	**Chondrule**	**Matrix**	**Chondrule**	**Matrix**
SiO_2	50.88	44.2	49.6	43.4	46.59	46.97
TiO_2	0.18	0.07	0.29	0.08	0.14	0.07
Al_2O_3	2.35	2.72	2.73	3.14	2.88	5.11
Cr_2O_3	0.39	0.27	0.95	0.4	0.46	0.45
FeO	13.21	21.01	14.95	20.77	14.85	15.48
MnO	0.34	0.42	0.4	0.37	0.31	0.24
MgO	28.44	28.2	29.64	28.51	30.21	26.19
CaO	3.23	1.52	0.65	1.91	2.89	3.3
Na_2O	0.7	0.92	0.65	0.86	0.96	1.56
K_2O	0.05	0.18	0.15	0.16	0.14	0.19
NiO	0.03	0.13	b.d.l.	0.31	0.21	0.16
SO_3	0.18	0.37	b.d.l.	0.08	0.35	0.28
Total	99.98	100.01	100.01	99.99	99.99	100

Note: b.d.l.—below detection limit.

Chondrule 1POP-0 consists of coarse idiomorphic olivine and low-Ca pyroxene (enstatite) grains; interstices between them are filled with xenomorphic plagioclase of oligoclase composition (Figure 1). Fine enstatite grains are overgrown with a thin high-Ca pyroxene rim. Chondrule 1POP-0 has no metallic and silicate rims. The meteorite matrix around the chondrule is highly shattered and fractured.

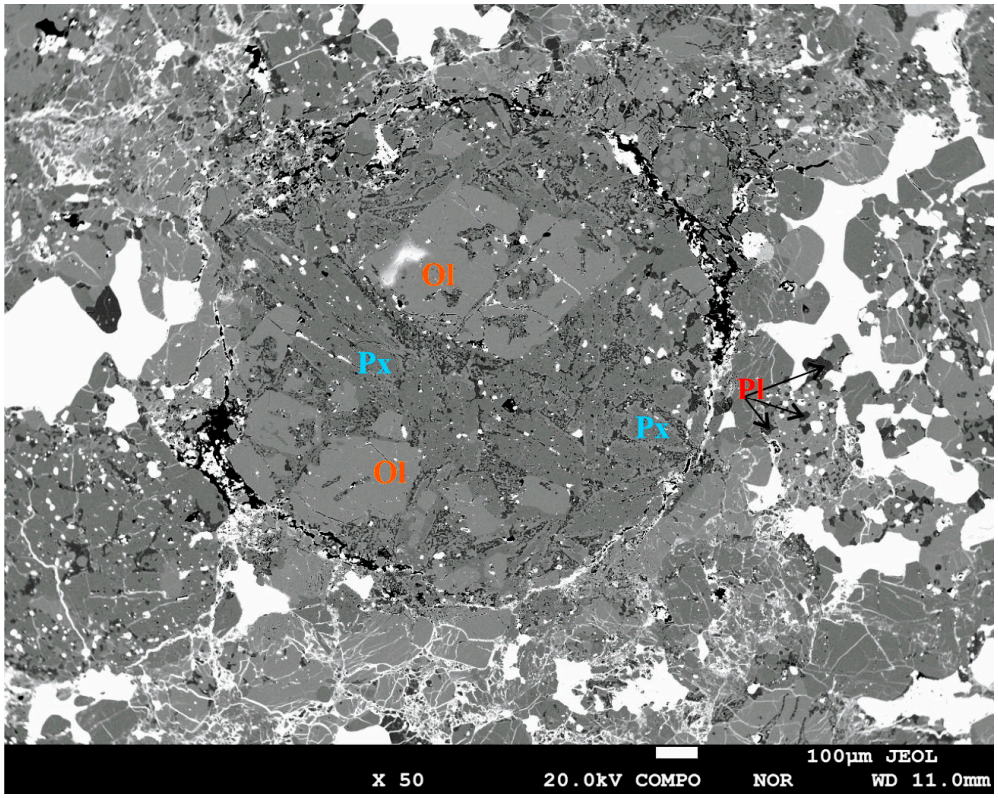

Figure 1. BSE image of 1POP-0 chondrule from the Kargapole meteorite. Ol–olivine, Px–pyroxene, Pl–plagioclase.

Olivine in the chondrule is present as coarse (200–300 µm) crystals, and is highly fractured and corroded. Olivine in the meteorite matrix near the chondrule occurs as fine (100–150 µm) highly fractured hypidiomorphic grains.

Olivine ($Fo_{79–80}$) in the center of the chondrule and olivine in the margin and the meteorite matrix practically do not differ in major element composition.

Olivine in the central portion of the chondrule contains high refractory (Zr, Y, Al, Ni, and Nb), moderately volatile (Sr and Ba) and REE concentrations (Table 2). Olivine at the chondrule rim has the lowest refractory Zr and Ca concentrations in comparison with olivine in the center of the meteorite chondrule and matrix. (Figure 2a).

Olivine in the meteorite is impoverished in trace elements relative to chondrite values. Concentrations of the volatile Ba and Rb in olivine from the center of the chondrule are closest to chondrite values. REE concentrations are highly fractionated in the olivine of the chondrule and the meteorite matrix; HREE prevail slightly ($0.1 < (Ce/Yb)_N < 0.4$) over LREE. A subchondritic Ca/Al ratio persists in the olivine of the chondrule, while no direct correlation between La and Yb is observed. In the trace element distribution pattern, the olivine pattern of the central portion is closest to chondrite values; the spectrum in other portions is practically sub-parallel, except for REE concentration. The trace element composition of olivine is generally consistent with olivine in unequilibrated chondrites [4].

Low-Ca pyroxene in chondrule 1POP-0 is present as fine (100–150 µm) hypidiomorphic grains occurring commonly on chondrule rims. Low-Ca pyroxene grains in the chondrule have a thin high-Ca pyroxene rim. Low-Ca pyroxene in the chondrule and matrix displays no compositional variations and corresponds to enstatite ($Fs_{18–20}$, Wo_1).

Low-Ca pyroxene in chondrule 1POP-0 differs by higher trace element concentrations, except for Ni, than pyroxene in the meteorite matrix (Table 2). Trace element concentrations, except for Al, LREE, Sr and Ba, in the pyroxene of the chondrule exceeds chondrite values. Low-Ca pyroxene in the chondrule retains a subchondritic Ca/Al ratio. Pyrox-

ene in the meteorite matrix is depleted of trace elements, except for Ti and V, relative to chondrite values.

REE concentrations in the pyroxene of the chondrule and the meteorite matrix exceed chondrite values, and HREE prevail over LREE ($0.08 < (Ce/Yb)_N < 0.15$). Low-Ca pyroxene from the meteorite matrix is similar in trace element concentration to pyroxene from the porphyric chondrules of unequilibrated chondrites. The pyroxene of the chondrule contains much higher refractory element and REE concentrations than pyroxenes in unequilibrated chondrites (Figure 2b).

Chondrule 1PO-2 is small and has a kamacite-taenite rim (Figure 3). It consists of olivine grains overgrowing low-Ca pyroxene along the chondrule rim. Interstices between chondrule grains are filled with plagioclase of oligoclase composition. The matrix around the chondrule is highly fractured.

Table 2. Major (measured by EPMA, in wt.%) and trace (measured by SIMS, in ppm) elements in silicate minerals of 1POP-0 chondrule from the Kargapole meteorite.

	1POP-0							
	Ol						**Px**	
	Center	**Center**	**Rim**	**Rim**	**Matrix**	**Matrix**	**Rim**	**Matrix**
SiO_2	39.27	39.26	39.32	39.56	39.36	39.27	54.99	55.79
TiO_2	b.d.l.	b.d.l.	b.d.l.	b.d.l.	0.02	0.01	0.44	0.25
Al_2O_3	b.d.l.	b.d.l.	b.d.l.	0.01	0.01	0.01	0.50	0.30
Cr_2O_3	0.02	0.01	b.d.l.	0.01	b.d.l.	b.d.l.	0.84	0.20
FeO	17.39	17.63	17.45	17.40	17.48	17.60	3.71	11.32
MnO	0.42	0.44	0.45	0.46	0.48	0.48	0.24	0.50
MgO	42.40	41.98	41.97	42.28	42.23	41.77	16.71	30.85
CaO	0.04	b.d.l.	0.02	0.03	b.d.l.	0.02	21.75	0.67
Na_2O								0.01
K_2O								0.01
NiO	b.d.l.	b.d.l.	b.d.l.	0.01	0.01	0.03	b.d.l.	b.d.l.
Total	99.53	99.33	99.21	99.77	99.59	99.19	99.18	99.90
Zr	0.77	0.95	0.08	0.10	0.14	0.22	33.8	0.70
Hf	0.04	0.04			0.03	0.04	1.06	0.08
Ca	4114	4588	3916	3866	4071	4104	39757	4655
Y	0.06	0.08	0.02	0.01	0.01	0.02	3.19	0.19
Al	1836	4660	712	79.6	73.1	65.1	5767	831
Ti	99.1	141	41.9	33.6	36.8	38.4	1763	991
Nb	0.18	0.22	0.03	0.03	0.03	0.05	0.80	0.11
La	0.02	0.02	0.02	0.01	0.01	0.01	0.13	0.01
Ce	0.04	0.03	0.03	0.02	0.02	0.04	0.41	0.02
Pr	0.01	b.d.l.		0.01		b.d.l.	0.09	b.d.l.
Nd	0.03	0.08	0.03	0.04		0.05	0.60	0.04
Sm		0.03	0.03		0.05		0.25	b.d.l.
Eu	0.01	0.05	b.d.l.	0.01	b.d.l.	b.d.l.	0.07	0.01
Gd	0.02	0.01			0.02	0.01	0.28	0.01
Dy		0.04		0.02		0.02	0.61	0.05
Er	0.03	0.04				0.02	0.41	0.04
Yb	0.05	0.02	0.02	0.02	0.04	0.04	0.74	0.07
Lu	0.01	0.01	0.01	0.01	0.01	0.01	0.07	0.02
Sr	2.32	5.98	0.37	0.18	0.23	0.25	6.62	0.67
Ba	1.25	2.70	0.30	0.14	0.26	0.32	1.87	0.48
V	15.8	18.7	18.6	15.8	16.9	18.4	175	49.8
Ni	24.1	31.5	26.2	18.9	36.2	25.3	20.7	71.0
Cr	486	362	400	395	406	412	1958	1178
Rb	1.04	2.66	0.88	1.00	1.06	0.93	2.25	0.57

Note: b.d.l.—below detection limit; blank—the element was not measured.

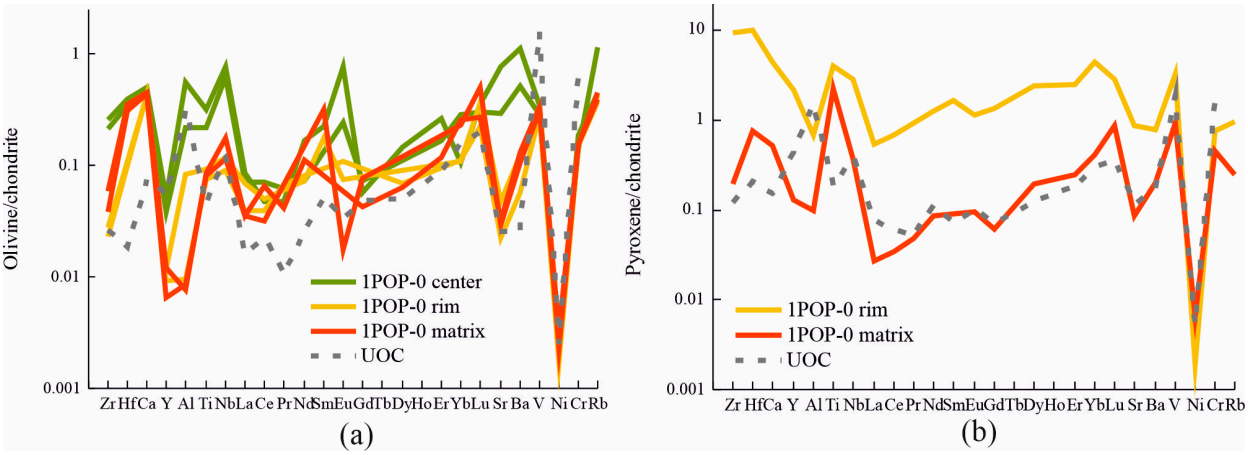

Figure 2. CI chondrite-normalized trace element patterns of olivine (**a**) and pyroxene (**b**) of 1POP-0 chondrule and matrix.

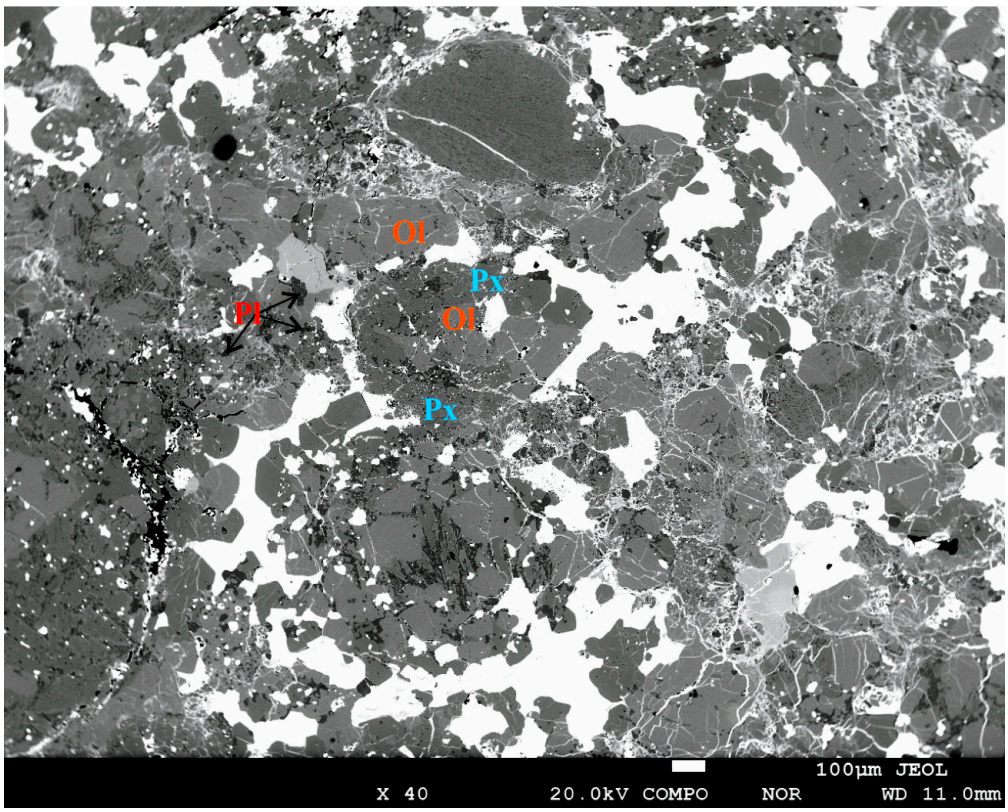

Figure 3. BSE image of 1PO-2 chondrule from the Kargapole meteorite.

Olivine in chondrule 1PO-2 occurs as fine (50–100 µm) hypidiomorphic grains. Outside the chondrule, olivine is present as coarse (300 µm) prismatic phenocrysts or fine highly shattered grains. Olivine in the chondrule and matrix is highly fractured.

Olivine in chondrule 1PO-2 and the meteorite matrix is forsteritic (Fo_{79}) and shows little variation in major element composition.

Coarse olivine from the central portion of the chondrule displays elevated refractory (except for Ti and Eu) and moderately volatile element concentrations (Table 3). Olivine in the central portion of the chondrules generally contains more incompatible (Nb, Sr, and Ba) elements than olivine in the meteorite matrix (Figure 4a).

Table 3. Major (measured by EPMA, in wt.%) and trace (measured by SIMS, in ppm) elements in silicate minerals of 1PO-2 chondrule from the Kargapole meteorite.

	1PO-2							
	Ol				**Px**		**Pl**	
	Center	**Center**	**Matrix**	**Matrix**	**Rim**	**Rim**	**Center**	**Matrix**
SiO_2	39.19	39.11	39.13	39.13	55.66	56.87	63.82	64.16
TiO_2	0.01	b.d.l.	0.02	0.03	0.16	0.20	0.08	0.01
Al_2O_3	b.d.l.	b.d.l.	b.d.l.	0.01	0.20	0.18	21.36	20.21
Cr_2O_3	0.02	0.01	b.d.l.	b.d.l.	0.08	0.10		
FeO	17.67	17.52	17.57	17.43	12.00	11.11	0.57	0.79
MnO	0.42	0.47	0.42	0.45	0.50	0.45		
MgO	41.85	42.12	42.01	42.06	30.89	30.75	0.10	0.32
CaO	0.02	0.01	0.02	0.01	0.52	0.81	2.94	2.72
Na_2O					b.d.l.	0.02	9.66	9.88
K_2O					b.d.l.	0.01	0.80	1.24
NiO	0.02	b.d.l.	b.d.l.	b.d.l.	0.03	b.d.l.		
Total	99.21	99.23	99.17	99.12	100	100	99.33	99.32
Zr	0.18	0.64	0.13	0.14	0.83	0.38	6.39	20.0
Hf		0.10			0.06	0.07	0.21	0.66
Ca	4001	4457	4054	3805	5495	5045		
Y	0.02	0.70	0.01	0.02	0.55	0.20	0.37	3.45
Al	180	1214	211	65.6	1376	671		
Ti	54.3	62.6	87.9	93.8	1104	1072	1259	999
Nb	0.07	0.08	0.02	0.02	0.23	0.04	1.74	0.86
La	0.02	0.16	0.01	0.02	0.08	0.01	0.14	0.62
Ce	0.02	0.50	0.03	0.03	0.15	0.02	0.15	1.35
Pr	0.01	0.06	b.d.l.	0.01	0.02	b.d.l.	0.01	0.23
Nd		0.42	0.04	0.04	0.11	b.d.l.	0.05	1.01
Sm		0.11		0.06	0.03	b.d.l.	0.04	0.47
Eu	0.01	0.01		0.01	0.01	0.01	0.55	0.68
Gd		0.25		0.06	0.09	0.04		0.31
Dy	0.02	0.20	0.02		0.06	0.04	0.02	0.51
Er		0.17	0.01	0.02	0.09	0.08	0.04	0.47
Yb	0.02	0.10	0.03	0.03	0.16	0.08	0.05	0.55
Lu		0.02	0.01	0.01	0.02	b.d.l.	0.01	0.07
Sr	0.75	3.44	0.35	0.32	3.83	0.12	82.2	93.1
Ba	0.49	2.09	0.19	0.28	1.80	0.08	34.9	37.4
V	16.1	18.6	17.6	16.5	50.9	47.2	177	83.9
Ni	74.2	281	66.0	41.9	1114	11.9		
Cr	441	397	382	380	923	952	9393	754
Rb	1.07	3.12	0.88	0.87	1.50	0.44	24.9	24.5

Note: b.d.l.—below detection limit; blank—the element was not measured.

HREE prevail slightly over LREE in olivine ($0.2 < (Ce/Yb)_N < 1.4$). The trace element distribution of olivine is generally unfractionated.

Low-Ca pyroxene in chondrule 1PO-2 occurs as xenomorphic aggregates on the chondrule rim and is present at the boundary between olivine and a kamacite-troilite rim. Some of the low-Ca pyroxene grains are highly shattered. Pyroxene in this chondrule is enstatite (Fs_{19}, Wo_1).

Low-Ca pyroxene of the chondrule is enriched in trace elements relative to chondrite values. A coarse pyroxene grain is much more enriched in REE and refractory elements than fine pyroxene grains in the chondrule (Figure 4b). HREE prevail over LREE ($0.07 < (Ce/Yb)_N < 0.2$).

Chondrule 1POP-4 consists of hypidiomorphic olivine and pyroxene grains; interstices between them are filled with plagioclase of oligoclase composition. The chondrule has no metallic rim, is highly porous and large. The meteorite matrix around the chondrule is highly shattered and fractured (Figure 5).

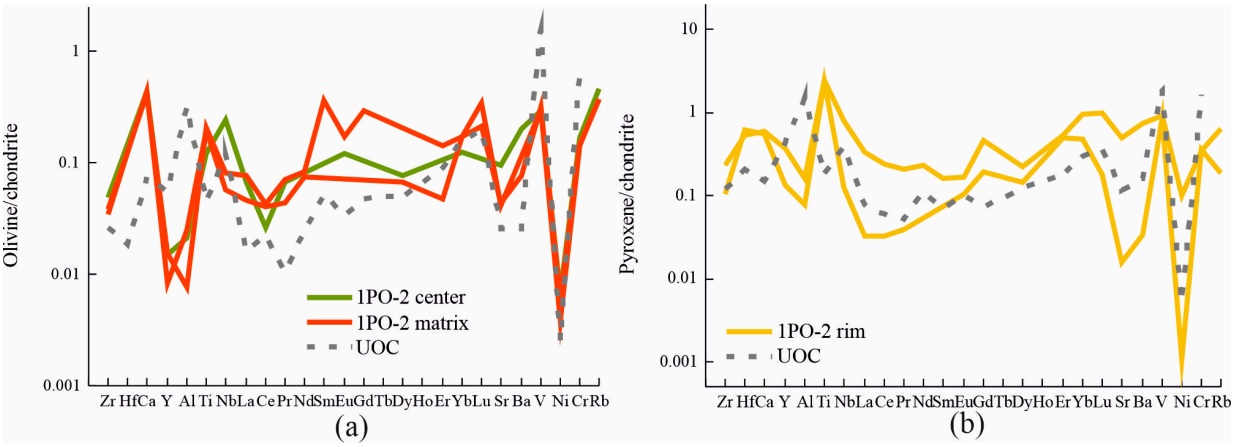

Figure 4. CI chondrite-normalized trace element patterns of olivine (**a**) and pyroxene (**b**) of 1PO-2 chondrule and matrix.

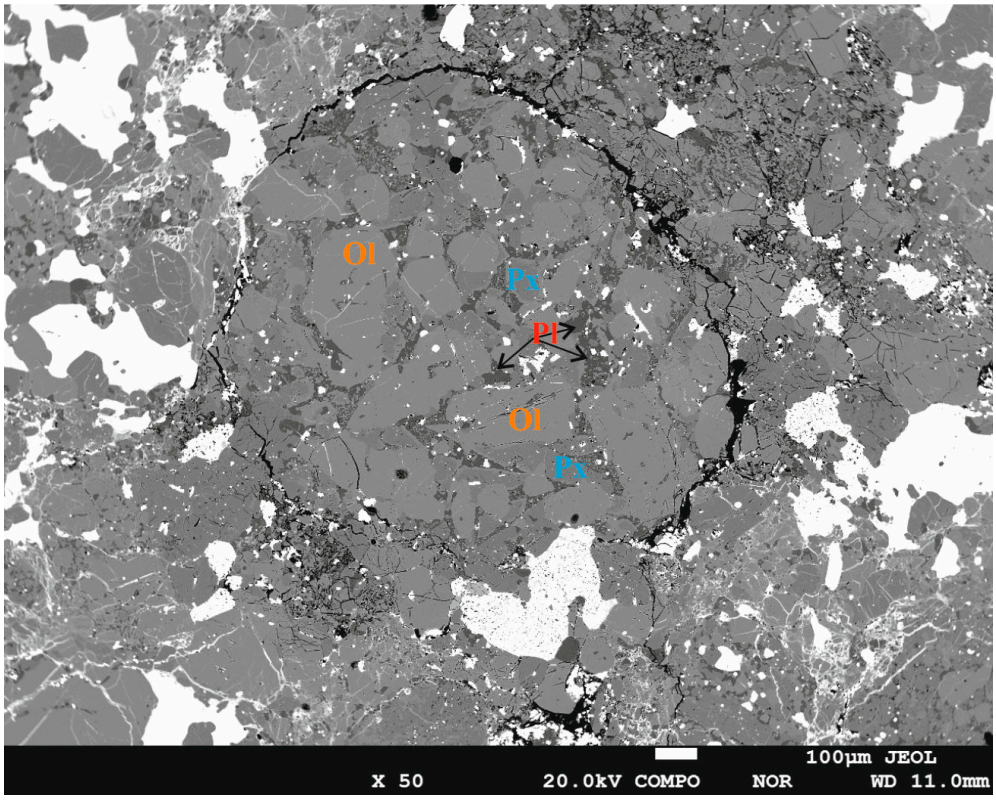

Figure 5. BSE image of 1POP-4 chondrule from Kargapole meteorite.

Olivine in the chondrule is present as coarse crystals of forsterite composition. Olivine grains in the chondrule and in the meteorite matrix are highly fractured. Olivine in the matrix occurs as xenomorphic aggregates. Olivine in the chondrule and in the meteorite matrix are forsteritic ($Fo_{79–80}$) and have similar major element compositions.

Olivine in the central portion of the chondrule contains less Al than olivine in the chondrule rims and the meteorite matrix. Olivines in the matrix is rich in Ce and Rb (Table 4).

Table 4. Major (measured by EPMA, in wt.%) and trace (measured by SIMS, in ppm) elements in silicate minerals of 1POP-4 chondrule from the Kargapole meteorite.

	1POP-4								
	Ol				Px				Pl
	Center	Center	Rim	Matrix	Center	Rim	Matrix	Matrix	Rim
SiO_2	39.11	39.27	39.20	39.32	56.27	55.63	56.29	55.86	64.39
TiO_2	0.01	b.d.l.	0.02	b.d.l.	0.21	0.21	0.10	0.19	0.05
Al_2O_3	0.02	b.d.l.	0.01	0.01	0.19	0.15	0.10	0.17	21.41
Cr_2O_3	b.d.l.	0.02	0.01	b.d.l.	0.14	0.10	0.10	0.14	
FeO	17.60	17.63	17.31	17.65	11.08	11.16	11.15	11.00	0.48
MnO	0.44	0.43	0.48	0.45	0.49	0.49	0.49	0.48	
MgO	41.82	41.93	42.00	41.99	30.67	30.61	30.99	30.77	0.12
CaO	0.02	b.d.l.	0.02	b.d.l.	0.60	0.63	0.80	0.83	2.49
Na_2O					b.d.l.	0.01	0.02	b.d.l.	10.05
K_2O					b.d.l.	b.d.l.	b.d.l.	b.d.l.	0.67
NiO	b.d.l.	b.d.l.	0.01	b.d.l.	0.02	b.d.l.	b.d.l.	b.d.l.	
Total	98.99	99.27	99.05	99.43	99.66	98.97	100	99.43	99.66
Zr	0.20	0.22	0.18	0.32	2.59	3.72	0.59	0.74	0.97
Hf		0.04	0.05		0.10	0.10	0.05	0.07	0.05
Ca	3516	3907	3437	4543	7740	4914	5084	5593	
Y	0.02	0.02	0.01	0.12	0.40	0.37	0.16	0.23	0.22
Al	46.2	50.8	219	313	722	1017	1872	891	
Ti	72.4	69.9	37.2	41.8	1018	1151	720	1053	427
Nb	0.01	0.01	0.07	0.13	0.11	0.38	0.08	0.14	0.11
La	0.01	0.01	0.01	0.04	0.02	0.04	0.01	0.02	0.11
Ce	0.02	0.04	0.02	0.20	0.05	0.07	0.04	0.04	0.08
Pr	0.01	0.01		0.01	0.01	0.01	0.01	b.d.l.	0.01
Nd	0.04		0.06		0.04	0.04	b.d.l.	0.03	0.05
Sm	0.04	0.06			0.02	0.02	0.02	0.03	
Eu	0.00	b.d.l.	0.01	0.01	b.d.l.	0.01	0.01	0.01	0.53
Gd		0.01	0.01		0.06	0.04	0.01	0.01	0.06
Dy	0.02			0.02	0.08	0.08	0.03	0.03	0.03
Er			0.02		0.10	0.05	0.02	0.03	0.05
Yb	0.04	0.02	0.02	0.02	0.14	0.13	0.06	0.15	0.01
Lu	0.02	0.01	0.01	0.01	0.01	0.02	0.01	0.01	b.d.l.
Sr	0.15	0.19	0.27	0.76	0.38	1.23	2.99	0.92	74.3
Ba	0.04	0.12	0.15	0.58	0.07	0.54	1.21	0.88	30.2
V	17.8	18.2	15.2	18.7	58.1	55.3	40.4	48.4	22.0
Ni	13.1	10.5	31.4	35.5	11.4	33.3	32.5	64.4	
Cr	358	385	339	436	1090	955	1085	973	183
Rb	0.88	0.88	0.76	3.33	0.44	1.21	1.38	1.38	21.62

Note: b.d.l.—below detection limit; blank—the element was not measured.

The trace element distribution pattern of olivine is practically undifferentiated (Figure 6a). Olivine is poorer in trace elements than in chondrites values. HREE prevail over LREE ($0.1 < (Ce/Yb)_N < 2.6$).

Low-Ca pyroxene in chondrule 1POP-4 occurs as fine hypidiomorphic grains evenly distributed over the chondrite region. In the matrix, pyroxene forms xenomorphic aggregates of various sizes. Low-Ca pyroxene in the chondrule and the meteorite matrix is homogeneous in major element composition and is identified as enstatite (Fs_{18}, Wo_1).

With respect to trace element composition, pyroxene from the central portion of the chondrule is enriched in refractory elements (Zr, Ca and Nb) in comparison to pyroxene from the meteorite matrix (Table 4). Low-Ca pyroxene from the matrix exhibits elevated moderately volatile incompatible element (Sr and Ba) concentrations (Figure 6b).

Trace element concentrations in pyroxene are close to chondrite values, except for REE. HREE clearly prevails over LREE ($0.01 < (Ce/Yb)_N < 0.16$). Low-Ca pyroxene from chondrule 1POP-4 is enriched in Ti and Nb with respect to chondrite values.

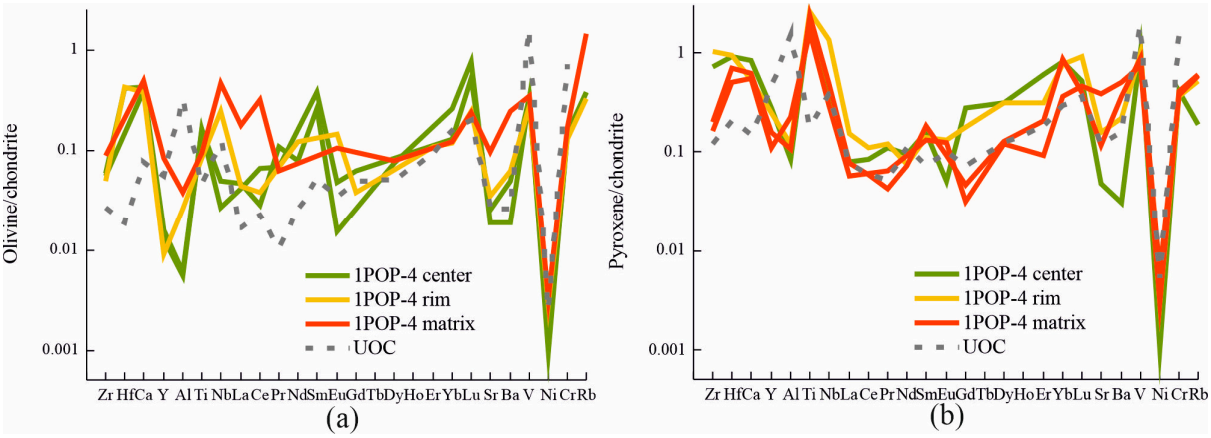

Figure 6. CI chondrite-normalized trace element patterns of olivine (**a**) and pyroxene (**b**) of 1POP-4 chondrule and matrix.

4. Discussion

Porphyritic chondrules in the Kargapole meteorite are generally impoverished relative to chondrite values. Their trace element distribution spectra are highly fractionated. One common feature of olivine from the chondrules is the dominance of HREE over LREE. High concentrations of refractory elements (Zr, Y, Ti, and Nb) and incompatible volatiles (Sr and Ba) is characteristic of olivine from chondrule 1POP-0. Olivine from chondrule 1PO-2 is enriched in Ni and REE and clearly shows a negative Eu-anomaly (Figure 7a).

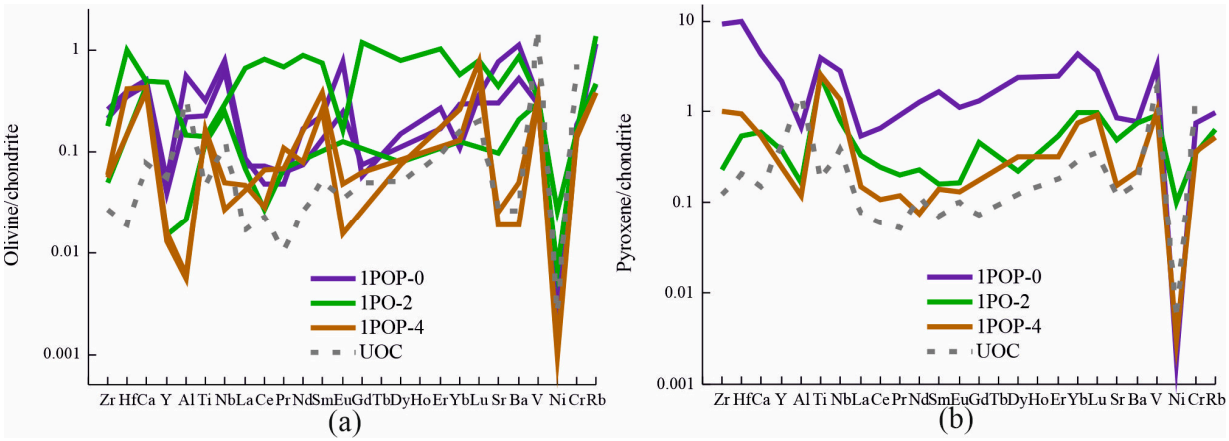

Figure 7. CI chondrite-normalized trace element patterns of olivine (**a**) and pyroxene (**b**) from chondrules.

The trace element distribution patterns in low-Ca pyroxene are sub-horizontal and similar to each other (Figure 7b). Trace element concentrations in pyroxene from Kargapole are close to chondrite values. Pyroxene from chondrule 1POP-0 is slightly enriched in trace elements relative to chondrules 1PO-2 and 1POP-4. In addition, pyroxene from chondrule 1POP-4 displays high Zr/V (Figure 8a) and low incompatible moderately volatile element (Sr and Ba) concentrations compared to other chondrules. Pyroxene from 1PO-2 is richer in Ni than pyroxenes from other chondrules of the meteorite (Table 3).

Olivine from the meteorite matrix is slightly richer in Yb (0.19 ppm on average) than olivine from the chondrules (0.13 ppm on average). Furthermore, olivine from the central portions of the chondrules shows higher Nb and Zr values than olivine from the chondrule rim and the meteorite matrix (Figure 8b).

Normalized olivine abundances from chondrules and the meteorite matrix are similar, differing only in a slight refractory element (Al, Ti, Nb) enrichment in olivine from chondrules and minimum Eu concentrations in olivine from the meteorite matrix (Figure 9a).

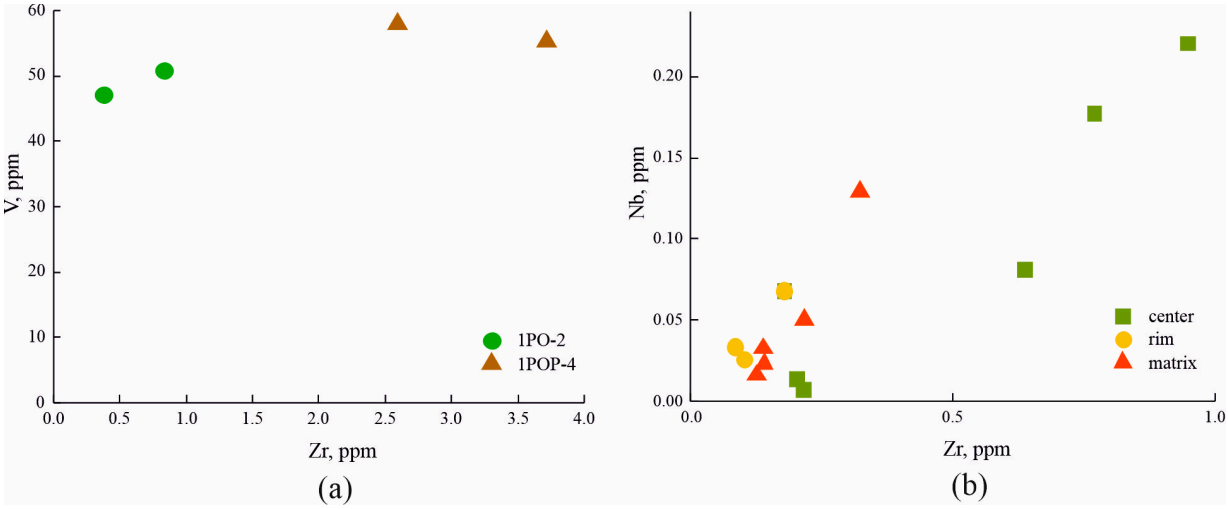

Figure 8. Trace element correlations (ppm) in chondrule pyroxene (**a**) and olivine (**b**) from the Kargapole meteorite.

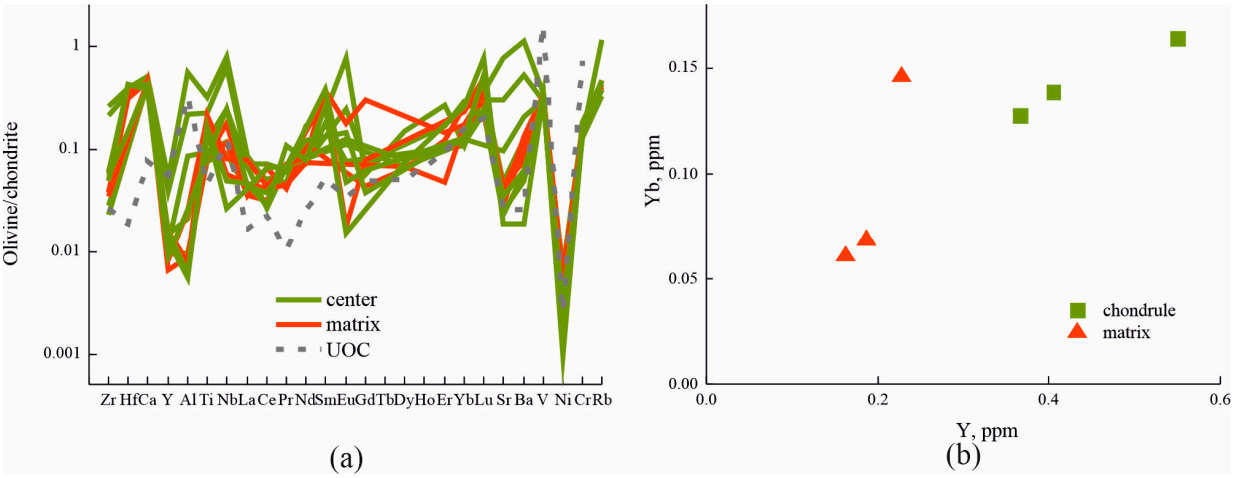

Figure 9. CI chondrite-normalized trace element patterns of olivine (**a**) from chondrules and the Kargapole meteorite matrix. (**b**) Yb and Y variation (ppm) in low-Ca pyroxene from chondrules of the Kargapole meteorite.

Low-Ca pyroxene from the chondrules displays high Y/Yb ratios (Figure 9b) and has higher refractory element concentrations than pyroxene from the meteorite matrix. Matrix pyroxene exhibits a negative Eu-anomaly. The refractory element concentrations in low-Ca pyroxene from chondrule rims occupy an intermediate position between enriched pyroxene from the chondrules center and depleted pyroxene from the meteorite matrix (Figure 10a).

Plagioclase in the Kargapole meteorite is richer in trace elements than olivine and low-Ca pyroxene from the meteorite (Tables 3 and 4). Trace element distribution patterns for plagioclase from the chondrules are very similar to and, for some elements, even higher than chondrite values (Figure 10b). In plagioclase from the matrix, trace element concentrations are higher than chondrite values.

Chondrite normalized trace element abundances for plagioclase from the meteorite are sub-horizontal and are similar to each other. Plagioclase from the Kargapole meteorite typically shows a positive Eu-anomaly and enrichment in Nb, Ti, Sr and Ba relative to chondrite values.

Trace element concentrations in plagioclase chondrules are similar to those of plagioclase from Renazzo unequilibrated carbonaceous chondrite, and the composition of

plagioclase from the meteorite matrix is approximately subparallel to plagioclase from Vigarano chondrite (Figure 10b).

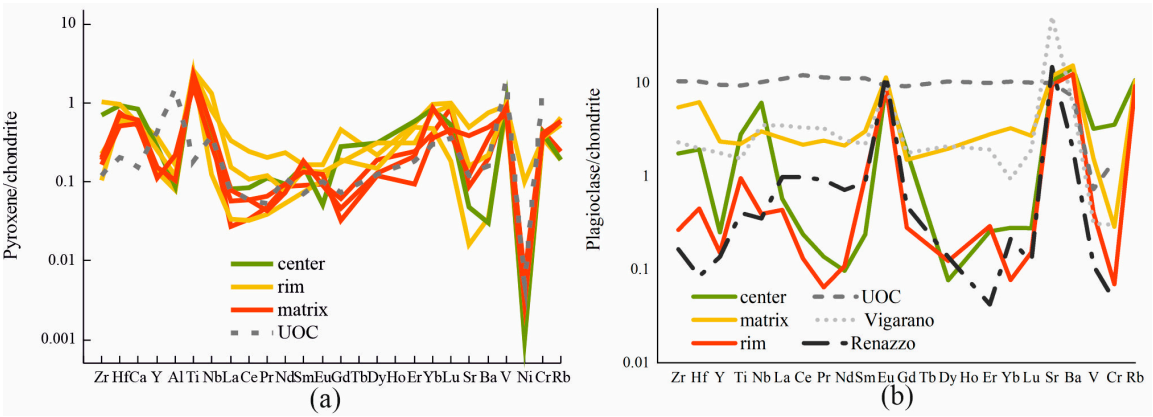

Figure 10. CI chondrite-normalized trace element patterns of low-Ca pyroxene (**a**) and plagioclase(**b**) from chondrules and the Kargapole meteorite matrix.

5. Conclusions

In spite of homogeneous major element concentrations, olivine and low-Ca pyroxene from Kargapole display considerable differences in trace element concentrations. Olivine and low-Ca pyroxene from chondrule POP-0 display elevated trace element concentrations relative to silicate minerals from chondrules PO-2 and POP-4 and from the meteorite matrix. Olivine and low-Ca pyroxene from the chondrules differ from those of the meteorite matrix in Nb and Zr concentrations in olivine and in Y/Yb ratios in low-Ca pyroxene.

Given the small database volume, elevated trace element concentrations in the silicate minerals of chondrule POP-0 relative to those of chondrules PO-2 and POP-4 suggest that the chondrule formed under special conditions. The enrichment of chondrule silicate minerals in refractory incompatible elements (Nb, Zr, Yb, and Y) relative to silicate minerals from the meteorite matrix suggests the formation of the chondrules at a higher cooling rate [32,33].

No considerable deviations in trace element concentrations in the olivine and pyroxene of the Kargapole meteorite from unequilibrated ordinary chondrites were detected, indicating a minor effect of impact metamorphism and terrestrial weathering on trace element mobilization in this meteorite.

Author Contributions: Conceptualization, S.S. and K.S.; methodology, S.S.; validation, O.G. and K.S.; formal analysis, K.S. and A.G.; investigation, K.S.; resources, S.S.; data curation, K.S.; writing—original draft preparation, K.S.; writing—review and editing, S.S.; visualization, K.S.; supervision, S.S.; project administration, A.G.; funding acquisition, S.S. All authors have read and agreed to the published version of the manuscript.

Funding: This study was supported by the government-financed research project FMUW-2022-0005 for the Institute of Precambrian Geology and Geochronology, Russian Academy of Sciences.

Informed Consent Statement: Not applicable.

Data Availability Statement: Data are contained within the article.

Acknowledgments: The authors wish to thank S.G. Simakin and E.V. Potapov (YaF FTIAN) for analytical work.

Conflicts of Interest: The authors declare no conflict of interest.

References

1. Dodd, R.T.; Hutchison, R. *Meteorites: A Petrologic, Chemical and Isotopic Synthesis*; Cambridge University Press: Cambridge, UK, 2004; p. 506.
2. Jacquet, E.; Alard, O.; Gounelle, M. Chondrule trace element geochemistry at the mineral scale. *Meteorit. Planet. Sci.* **2012**, *47*, 1695–1714. [CrossRef]
3. Jacquet, E.; Alard, O.; Gounelle, M. The formation conditions of enstatite chondrites: Insights from trace element geochemistry of olivine-bearing chondrules in Sahara 97096 (EH3). *Meteorit. Planet. Sci.* **2015**, *50*, 1624–1642. [CrossRef]
4. Jacquet, E.; Alard, O.; Gounelle, M. Trace element geochemistry of ordinary chondrite chondrules: The type I/type II chondrule dichotomy. *Geochim. Cosmochim. Acta* **2015**, *155*, 47–67. [CrossRef]
5. Varela, M.E.; Sylvester, P.; Brandstätter, F.; Engler, A. Nonporphyritic chondrules and chondrule fragments in enstatite chondrites: Insights into their origin and secondary processing. *Meteorit. Planet. Sci.* **2015**, *50*, 1338–1361. [CrossRef]
6. Varela, M.E.; Sylvester, P.; Engler, A.; Kurat, G. Nonporphyritic chondrules from equilibrated Rumuruti and ordinary chondrites: Chemical evidence of secondary processing. *Meteorit. Planet. Sci.* **2012**, *47*, 1537–1557. [CrossRef]
7. Hezel, D.C.; Palme, H. The chemical relationship between chondrules and matrix and the chondrule matrix complementarity. *Earth Planet. Sci. Lett.* **2010**, *294*, 85–93. [CrossRef]
8. Sukhanova, K.G.; Kuznetsov, A.B.; Galankina, O.L. Features of olivine crystallization in ordinary chondrites (Saratov meteorite): Geochemistry of trace and rare earth elements. *J. Min. Inst.* **2022**, *254*, 149–157. [CrossRef]
9. Sukhanova, K.G.; Kuznetsov, A.B.; Skublov, S.G. Geochemical Features of Chondrules from Orlovka Meteorite (H5): Evidence of Melting Precursors. *Dokl. Earth Sci.* **2022**, *504*, 28–33. [CrossRef]
10. Sukhanova, K.G.; Skublov, S.G.; Galankina, O.L.; Obolonskaya, E.V.; Kotova, E.L. Trace element composition of silicate minerals in the chondrules and matrix of the Buschhof meteorite. *Geochem. Int.* **2020**, *58*, 1321–1330. [CrossRef]
11. Sukhanova, K.G.; Skublov, S.G.; Galankina, O.L.; Obolonskaya, E.V.; Kotova, E.L. Trace element composition of silicate minerals in the porphyritic and nonporphyritic chondrules of Elenovka (L5) and Knyahinya (L/LL5) meteorites. *Geochemistry* **2020**, *82*, 125920. [CrossRef]
12. Ovchinnikov, L.N.; Yudin, I.A. Study of the stone meteorite Kargapole. *Meteoritica* **1966**, *27*, 76–88.
13. Sharygin, V.V.; Kolisnichenko, S.V. Yaratkulovo—A new H-chondrite in the Urals: Mineralogical data. *Mineralogy* **2017**, *1*, 3–15.
14. Kharitonova, V.Y. The chemical composition of the chondrites Kaande, Kargopole, Dimmit, Chico And New Almelo from the collection of the meteorite committee of the Academy of Sciences of the USSR. *Meteoritica* **1969**, *29*, 91–93.
15. Ovchinnikov, L.N.; Maksenkov, V.G. Thermoluminescence of some stony meteorites. *Meteoritica* **1966**, *27*, 58–62.
16. Guskova, E.G. On the magnetization of stony meteorites represented by finds. *Meteoritica* **1988**, *47*, 137–142.
17. Koroteev, V.A.; Petrishcheva, V.G.; Loginov, V.N.; Yudin, I.A. Thermal studies of chondrites. *Meteoritica* **1989**, *48*, 121–123.
18. Erokhin, Y.V.; Berzin, S.V.; Ivanov, K.S.; Burlakov, E.V.; Kleimenov, D.A. Pentlandite from some H-type Ural chondrites. *Bull. Ural. Branch Russ. Mineral. Soc.* **2015**, *12*, 40–45.
19. Erokhin, Y.V.; Berzin, S.V.; Khiller, V.V.; Ivanov, K.S. Pentlandite from ordinary chondrites of the Urals. *Lithosphere* **2016**, *3*, 139–146.
20. Erokhin, Y.V.; Koroteev, V.A.; Khiller, V.V.; Burlakov, E.V.; Ivanov, K.S.; Kleimenov, D.A. The Kargapole meteorite: New data on mineralogy. *Dokl. Earth Sci.* **2017**, *477*, 1441–1444. [CrossRef]
21. Sukhanova, K.G.; Kuznetsov, A.B.; Skublov, S.G.; Galankina, O.L. Evaluation of thermal metamorphism temperature of equilibrated ordinary chondrites. *Geodyn. Tectonophys.* **2022**, *13*, 0618. (In Russian) [CrossRef]
22. Batanova, V.; Suhr, G.; Sobolev, A. Origin of geochemical heterogeneity in the mantle peridotites from the Bay of Islands ophiolite, Newfoundland, Canada: Ion probe study of clinopyroxenes. *Geochim. Cosmochim. Acta* **1998**, *62*, 853–866. [CrossRef]
23. Nosova, A.; Narkisova, V.; Sazonova, L.; Simakin, S. Minor elements in clinopyroxene from Paleozoic volcanics of the Tagil island arc in the Central Urals. *Geochem. Int.* **2002**, *40*, 219–232.
24. Portnyagin, M.; Almeev, R.; Matveev, S.; Holtz, F. Experimental evidence for rapid water exchange between melt inclusions in olivine and host magma. *Earth Planet. Sci. Lett.* **2008**, *272*, 541–552. [CrossRef]
25. Jochum, K.P.; Dingwell, D.B.; Rocholl, A.; Stoll, B.; Hofmann, A.W.; Becker, S.; Besmehn, A.; Bessette, D.; Dietze, H.J.; Dulski, P. The preparation and preliminary characterisation of eight geological MPI-DING reference glasses for in-situ microanalysis. *Geostand. Newsl.* **2000**, *24*, 87–133. [CrossRef]
26. Bottazzi, P.; Ottolini, L.; Vannucci, R.; Zanetti, A. An accurate procedure for the quantification of rare earth elements in silicates. In *SIMS 9th Proceedings*; Wiley: New York, NY, USA, 1994; pp. 927–930.
27. Jochum, K.P.; Stoll, B.; Herwig, K.; Willbold, M.; Hofmann, A.W.; Amini, M.; Aarburg, S.; Abouchami, W.; Hellebrand, E.; Mocek, B. MPI-DING reference glasses for in situ microanalysis: New reference values for element concentrations and isotope ratios. *Geochem. Geophys. Geosystems* **2006**, *7*, 1–44. [CrossRef]
28. Rocholl, A.B.; Simon, K.; Jochum, K.P.; Bruhn, F.; Gehann, R.; Kramar, U.; Luecke, W.; Molzahn, M.; Pernicka, E.; Seufert, M. Chemical Characterisation of NIST Silicate Glass Certified Reference Material SRM 610 by ICP-MS, TIMS, LIMS, SSMS, INAA, AAS and PIXE. *Geostand. Newsl.* **1997**, *21*, 101–114. [CrossRef]
29. Ottolini, L.; Bottazzi, P.; Vannucci, R. Quantification of lithium, beryllium, and boron in silicates by secondary-ion mass spectrometry using conventional energy filtering. *Anal. Chem.* **1993**, *65*, 1960–1968. [CrossRef]
30. Palme, H.; Lodders, K.; Jones, A. Solar system abundances of the elements. In *Treatise on Geochemistry*, 2nd ed.; Holland, H.D., Turekian, K.K., Eds.; Elsevier: Oxford, UK, 2014; Volume 2, pp. 15–36.

31. Wlotzka, F. A weathering scale for the ordinary chondrites. *Meteoritics* **1993**, *28*, 460.
32. Cherniak, D.J.; Dimanov, A. Diffusion in Pyroxene, Mica and Amphibole. *Rev. Mineral. Geochem.* **2010**, *72*, 641–690. [CrossRef]
33. Cherniak, D.J. REE diffusion in olivine. *Am. Mineral.* **2010**, *95*, 362–368. [CrossRef]